Vietnam Journal of Mechanics, VAST, Vol. 44, No. 1 (2022), pp. 83 – 95
DOI: https://doi.org/10.15625/0866-7136/16852

STRENGTH AND FATIGUE ANALYSIS OF PERIODIC PERFORATED MATERIALS USING THE COMPUTATIONAL HOMOGENIZATION AND ES-FEM APPROACHES

Phuong H. Nguyen[1], **Canh V. Le**[1,*], **Phuc L.H. Ho**[1]
[1]*Department of Civil Engineering, International University, Vietnam National University Ho Chi Minh City, Vietnam*
[*]E-mail: lvcanh@hcmiu.edu.vn

Received: 30 December 2021 / Published online: 30 March 2022

Abstract. This paper presents a computational homogenization shakedown analysis of periodic perforated materials with von Mises matrices. The plastic behaviors of the perforated materials under cyclic macroscopic loads are studied by means of kinematic shakedown theorem and computational homogenization method. The kinematic micro-fields are approximated by the edge-based smoothed finite element method. The resulting large-scale optimization problem is efficiently solved by using conic solver, enabling a large number of points on the macroscopic strength and fatigue surface to be calculated rapidly. The effects of the hole's shape and size on the overall strength and fatigue domains are also investigated.

Keywords: shakedown analysis, computational homogenization, overall plastic properties, ES-FEM.

1. INTRODUCTION

The overall properties of heterogeneous materials can be determined by solving a boundary-value problem formulated at micro-level. At a material/integration point of macro-structures, a representative volume element (RVE) or unit cell is assigned and macro-stresses or -strains are applied on its boundaries as external loads [1–3]. In order to capture the effects of the mechanical and geometrical properties of micro-structures and their interaction at micro-level on the overall plastic behaviors, shakedown analysis of micro-structures has been developed by using the shakedown theorems in combination with the homogenization theory [4–7]. In these formulations, the microscopic periodic displacement fields are approximated using the finite element method. As a result, the plastic dissipation function involves both the macroscopic strains and the micro degree of freedoms, and hence efforts must be paid to treat the objective function, particularly when using the direct iterative optimization algorithm [6,7]. Moreover, there is a need to

reformulate the stiffness matrix in order calculate the fictitious elastic stresses [4,5]. It is, therefore, worthwhile to improve the performance of this method.

In this paper, the shakedown formulation presented in [4–7] is reformulated in terms of total micro-displacement. The obtained problem is closely similar to the formulation defined for the structures, and hence it is convenient to extend advanced techniques used shakedown analysis of structures to that of micro-structures. The total micro-displacements are approximated using the edge-based smoothed finite element method (ES-FEM). The computational homogenization method [1–3] is used to calculate the fictitious elastic stresses and to enforce periodic boundary conditions which are constraints of the microscopic kinematic shakedown problem. The discrete formulation is then transformed into a conic optimization problem, being solved by using the primal-dual interior point algorithm implemented in Mosek package. Circular and rectangular perforated materials are examined to determine its macroscopic strength and fatigue criteria. The effects of the hole's shape and size on the overall plastic properties are also reported.

2. KINEMATIC HOMOGENISED SHAKEDOWN ANALYSIS OF MICRO-STRUCTURES

Consider a elastic-perfectly plastic representative volume element (RVE) of area Ω_m and boundary Γ under cyclic macroscopic stress $\mathbf{\Sigma}$ (associated with macroscopic strain $\mathbf{E}$). According to the homogenization theory, the microscopic stresses and strain rates are linked with macroscopic quantities by the average relations as

$$\mathbf{\Sigma} = \langle \boldsymbol{\sigma} \rangle,\ \mathbf{E} = \langle \boldsymbol{\epsilon} \rangle,\ \Delta\mathbf{E} = \langle \Delta\boldsymbol{\epsilon} \rangle,\ \text{with } \langle f \rangle = \frac{1}{|\Omega_m|}\int_{\Omega_m} f \, \mathrm{d}\Omega_m \tag{1}$$

where $\boldsymbol{\sigma}$ and $\boldsymbol{\epsilon}$ are respectively the microscopic stress and strain fields, $\Delta\boldsymbol{\epsilon}$ is the accumulative microscopic plastic strain fields, $\Delta\mathbf{E}$ is the accumulative macroscopic plastic strains and ∇ is the linear differential operator.

Let $\boldsymbol{\sigma}^e(\mathbf{x}, t)$ be the fictitious elastic stress response of the RVE to macroscopic stresses $\lambda^+\mathbf{\Sigma}$, over a period of time ($\mathbf{x} \in \Omega, t \in [0, T]$). The kinematic shakedown analysis of periodic media [4–7] can be re-expressed in terms of the total microscopic displacement as

$$\begin{aligned} \lambda^+ \quad = \quad & \min_{\boldsymbol{\epsilon}^p, \Delta\mathbf{u}, \Delta\mathbf{E}} \int_0^T \int_{\Omega_m} \mathcal{D}(\boldsymbol{\epsilon}^p)\, \mathrm{d}\Omega_m \mathrm{d}t \\ & \text{s.t} \begin{cases} \displaystyle\int_0^T \int_{\Omega_m} \boldsymbol{\sigma}^{eT}(\mathbf{x}, t)\boldsymbol{\epsilon}^p \, \mathrm{d}\Omega_m \mathrm{d}t = 1 \\ \Delta\boldsymbol{\epsilon} = \displaystyle\int_0^T \boldsymbol{\epsilon}^p \, \mathrm{d}t = \frac{1}{2}[\nabla\Delta\mathbf{u} + (\nabla\Delta\mathbf{u})^T] & \text{in } \Omega_m \\ \Delta\mathbf{u}(\mathbf{x}) - \Delta\mathbf{E}\cdot\mathbf{x} & \text{periodic on } \Gamma \end{cases} \end{aligned} \tag{2}$$

where $\mathcal{D}(\boldsymbol{\epsilon}^p)$ is the plastic dissipation power and $\Delta\mathbf{u}$ is the accumulative displacements. Note that at each instant during the time cycle t, the plastic strain rates $\boldsymbol{\epsilon}^p$ may be not compatible, but the plastic strain accumulated over the cycle $\Delta\boldsymbol{\epsilon}$ must be compatible.

Matrices of micro-materials are isotropic and governed by the von Mises failure criterion in plane stress as

$$\psi(\boldsymbol{\sigma}) = \boldsymbol{\sigma}^T \mathbf{Y} \boldsymbol{\sigma} \leq 1 \tag{3}$$

where $\mathbf{Y}$ is the matrix containing the strength properties of the micro-materials and given by

$$\mathbf{Y} = \frac{1}{\sigma_p^2} \begin{bmatrix} 1 & -0.5 & 0 \\ -0.5 & 1 & 0 \\ 0 & 0 & 3 \end{bmatrix} \tag{4}$$

with σ_p is the reference yield stress.

The plastic dissipation power associated with the von Mises failure criterion can be formulated in terms of the total microscopic strain rates as

$$\mathcal{D}\left(\boldsymbol{\epsilon}^p\right) = \sqrt{\boldsymbol{\epsilon}^{pT} \mathbf{Y}^{-1} \boldsymbol{\epsilon}^p} \tag{5}$$

Now, the kinematic homogenised shakedown analysis of periodic media governed the von Mises failure criterion becomes

$$\begin{aligned} \lambda^+ \quad = \quad & \min_{\boldsymbol{\epsilon}^p, \Delta\mathbf{u}, \Delta\mathbf{E}} \int_0^T \int_{\Omega_m} \sqrt{\boldsymbol{\epsilon}^{pT} \mathbf{Y}^{-1} \boldsymbol{\epsilon}^p}\, \mathrm{d}\Omega_m \mathrm{d}t \\ & \text{s.t} \begin{cases} \displaystyle\int_0^T \int_{\Omega_m} \boldsymbol{\sigma}^{eT}(\mathbf{x}, t) \boldsymbol{\epsilon}^p \, \mathrm{d}\Omega_m \mathrm{d}t = 1 \\ \Delta\boldsymbol{\epsilon} = \displaystyle\int_0^T \boldsymbol{\epsilon}^p \, \mathrm{d}t = \frac{1}{2}[\nabla\Delta\mathbf{u} + (\nabla\Delta\mathbf{u})^T] & \text{in } \Omega_m \\ \Delta\mathbf{E} = \langle \Delta\boldsymbol{\epsilon} \rangle \\ \Delta\mathbf{u}(\mathbf{x}) - \Delta\mathbf{E} \cdot \mathbf{x} & \text{periodic on } \Gamma \end{cases} \end{aligned} \tag{6}$$

The solution of the problem (6) is the smaller one of low-cycle fatigue limit and ratcheting limit.

In numerical analysis, the time integration in the problem (6) must be numerically calculated due to the determination of plastic strains over a loading cycle would be difficult. To this end, the load domain in the space of the macroscopic stresses $\boldsymbol{\Sigma}$ can be expressed as

$$\boldsymbol{\Sigma} = \begin{bmatrix} \mu_1 \Sigma_{11} & \mu_2 \Sigma_{22} & \mu_3 \Sigma_{33} & \mu_4 \Sigma_{12} & \mu_5 \Sigma_{23} & \mu_6 \Sigma_{31} \end{bmatrix}^T \tag{7}$$

where $\mu_i^- \leq \mu_i \leq \mu_i^+$, $i = 1, 2, \ldots, 6$, are the amplifying factors that vary independently.

Using the two convex-cycle theorems [8], shakedown analysis can be performed only at the vertices of the convex polyhedral loading domain defined by (7). The problem (6) can be then reformulated as

$$\lambda^+ = \min_{\boldsymbol{\epsilon}_k^p,\,\Delta\mathbf{u},\,\Delta\mathbf{E}} \sum_{k=1}^{\mathcal{N}_L} \int_{\Omega_m} \sqrt{\boldsymbol{\epsilon}_k^{pT}\mathbf{Y}^{-1}\boldsymbol{\epsilon}_k^p}\,\mathrm{d}\Omega_m$$

$$\text{s.t}\begin{cases} \displaystyle\sum_{i=1}^{\mathcal{N}_L} \int_{\Omega_m} \boldsymbol{\sigma}_k^{eT}\boldsymbol{\epsilon}_k^p\,\mathrm{d}\Omega_m = 1 \\ \Delta\boldsymbol{\epsilon} = \displaystyle\sum_{k=1}^{\mathcal{N}_L} \boldsymbol{\epsilon}_k^p = \frac{1}{2}[\nabla\Delta\mathbf{u} + (\nabla\Delta\mathbf{u})^T] \quad \text{in } \Omega_m \\ \Delta\mathbf{E} = \langle\Delta\boldsymbol{\epsilon}\rangle \\ \Delta\mathbf{u}(\mathbf{x}) - \Delta\mathbf{E}\cdot\mathbf{x} \qquad\qquad \text{periodic on } \Gamma \end{cases} \tag{8}$$

where $\mathcal{N}_L$ is the number of vertices of the convex polyhedral load domain.

In order to obtain numerical solutions of the problem (8), the accumulative displacement field must be approximated using a numerical method. In this paper, the edge-based smoothed finite element method is used and recalled in the following section.

3. EDGE-BASED SMOOTHED FINITE ELEMENT METHOD

In the edge-based smoothed finite element method (ES-FEM) [9], the problem domain is divided into smoothing domains based on edges of elements such that $\Omega \approx \bigcup_{k=1}^{\mathcal{N}_{ed}} \Omega_k$ and $\Omega^i \cap \Omega^j = \oslash$ for $i \neq j$, in which $\mathcal{N}_{ed}$ is the total number of elemental edges in the problem domain. The shape functions used in FEM and ES-FEM are identical. However, the ES-FEM uses smoothed strains over local smoothing domains, instead of using compatible strains as in FEM. Employing triangular three-node elements, these local smoothing cells are generated based on elemental edges as illustrated in Fig. 1.

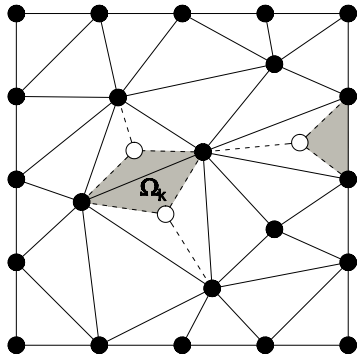

Fig. 1. Triangular elements (solid lines) and the edge-based smoothing domains (shaded areas)

Smoothed strains are determined based on the compatible strains by

$$\tilde{\boldsymbol{\epsilon}}_k^h = \int_{\Omega_k} \boldsymbol{\epsilon}^h(\mathbf{x})\phi_k(\mathbf{x})\mathrm{d}\Omega = \int_{\Omega_k} \nabla\mathbf{u}^h(\mathbf{x})\phi_k(\mathbf{x})\mathrm{d}\Omega \tag{9}$$

where $\nabla\mathbf{u}^h$ are the compatible strains of the approximation displacements $\mathbf{u}^h$, and $\phi_k(\mathbf{x})$ is a smoothing function given by

$$\int_{\Omega_k} \phi_k(\mathbf{x})\,\mathrm{d}\Omega = 1 \tag{10}$$

For computational convenience, the smoothing function ϕ_k is chosen as

$$\phi_k(\mathbf{x}) = \begin{cases} 1/A_k, \ \mathbf{x} \in \Omega_k \\ 0, \ \text{otherwise} \end{cases} \tag{11}$$

where A_k is the area of the smoothing cell Ω_k, and is determined by

$$A_k = \int_{\Omega_k} \mathrm{d}\Omega = \frac{1}{3} \sum_{j=1}^{\mathcal{N}_e^k} A_e^j \tag{12}$$

where $\mathcal{N}_e^k$ is the number of elements associated with the edge k and A_e^j is the area of the j^{th} element associated with the edge k.

The smoothed strains can be then determined by

$$\tilde{\boldsymbol{\epsilon}}_k^h = \tilde{\mathbf{B}}_k \mathbf{d}_k \tag{13}$$

where $\mathbf{d}_k$ is the displacement vector containing degree of freedoms of the nodes of edge k, and $\tilde{\mathbf{B}}_{kj}(j = 1, 2)$ are the strain-displacement matrices calculated by

$$\tilde{\mathbf{B}}_{kj} = \begin{bmatrix} \tilde{N}_{1,x}^{kj} & 0 & \dots & \tilde{N}_{n,x}^{kj} & 0 \\ 0 & \tilde{N}_{1,y}^{kj} & \dots & 0 & \tilde{N}_{n,y}^{kj} \\ \tilde{N}_{1,y}^{kj} & \tilde{N}_{1,x}^{kj} & \dots & \tilde{N}_{n,y}^{kj} & \tilde{N}_{n,x}^{kj} \end{bmatrix} \tag{14}$$

where $\tilde{N}_{I,\alpha}^{kj}$ is the smoothed version of shape function derivative, see [10] for more details.

4. ES-FEM BASED KINEMATIC HOMOGENISED SHAKEDOWN ANALYSIS

The smoothed accumulative strains in micro-problem are approximated using the ES-FEM method and linked to the macroscopic accumulative strains by

$$\Delta\mathbf{E} = \frac{1}{|\Omega_m|} \int_{\Omega_m} \Delta\boldsymbol{\epsilon}^h \, \mathrm{d}\Omega_m = \frac{1}{|\Omega_m|} \sum_{k=1}^{\mathcal{N}_{ed}} A_k \tilde{\mathbf{B}}_k \Delta\mathbf{d} \tag{15}$$

The key differences between the kinematic shakedown analysis formulated for the RVE and that of macro-structures are the periodic conditions for the accumulative displacements and the averaging relations for the accumulative strains. These constraints can be conveniently performed within the framework of the computational homogenization method [2]. The periodic condition for each pair $\{\mathbf{x}^+, \mathbf{x}^-\}$ of the RVE boundary is

$$\Delta\mathbf{u}^h(\mathbf{x}^+) - \Delta\mathbf{E} \cdot \mathbf{x}^+ = \Delta\mathbf{u}^h(\mathbf{x}^-) - \Delta\mathbf{E} \cdot \mathbf{x}^- \tag{16}$$

which can be then expressed in the matrix form as [11]

$$\mathbf{A}_1 \Delta\mathbf{d} + \mathbf{A}_2 \Delta\mathbf{E} = 0 \tag{17}$$

in which $\mathbf{A}_1$ and $\mathbf{A}_2$ are the link-topology matrices, consisting of $\{0, 1, -1\}$ only.

Employing the smoothed accumulative displacement and strain fields, the homogenized formulation for kinematic shakedown analysis of perforated materials governed von Mises failure criterion in plane stress can be discretized as

$$\begin{aligned}
\lambda^{+} \quad = \quad & \min_{\boldsymbol{\epsilon}^{p}_{ki},\,\Delta\mathbf{u},\,\Delta\mathbf{E}} \sum_{i=1}^{\mathcal{N}_L}\sum_{k=1}^{\mathcal{N}_{ed}} A_k \sqrt{\boldsymbol{\epsilon}^{pT}_{ki}\mathbf{Y}^{-1}\boldsymbol{\epsilon}^{p}_{ki}} \\
& \text{s.t} \begin{cases}
\displaystyle\sum_{i=1}^{\mathcal{N}_L}\sum_{k=1}^{\mathcal{N}_{ed}} A_k \boldsymbol{\sigma}^{eT}_{ki}\boldsymbol{\epsilon}^{p}_{ki} = 1 \\
\Delta\boldsymbol{\epsilon}^{h}_{k} = \displaystyle\sum_{i=1}^{\mathcal{N}_L} \boldsymbol{\epsilon}^{p}_{ki} = \tilde{\mathbf{B}}_k \Delta\mathbf{d}, \qquad k = 1,\,2,\ldots,\mathcal{N}_{ed} \\
\Delta\mathbf{E} = \dfrac{1}{|\Omega_m|}\displaystyle\sum_{k=1}^{\mathcal{N}_{ed}} A_k \tilde{\mathbf{B}}_k \Delta\mathbf{d} \\
\mathbf{A}_1\Delta\mathbf{d} + \mathbf{A}_2\Delta\mathbf{E} = 0
\end{cases}
\end{aligned} \tag{18}$$

The objective function of the problem (18) is cast in a form involving a sum of norms as

$$\mathcal{D}^{ESFEM} = \sum_{i=1}^{\mathcal{N}_L}\sum_{k=1}^{\mathcal{N}_{ed}} A_k \left|\left|\mathbf{J}^{\mathrm{T}}\boldsymbol{\epsilon}^{p}_{ki}\right|\right| \tag{19}$$

where $||\cdot||$ is the Euclidean norm, i.e, $||\mathbf{v}|| = (\mathbf{v}^T\mathbf{v})^{1/2}$, and $\mathbf{J}$ is the so-called Cholesky factor of $\mathbf{Y}^{-1}$.

Defining additional variables $\boldsymbol{\chi}_{ki}$ as

$$\boldsymbol{\chi}_{ki} = \mathbf{J}^{\mathrm{T}}\boldsymbol{\epsilon}^{p}_{ki} \tag{20}$$

The problem (18) can be then cast in the form of a standard conic programming problem

$$\begin{aligned}
\lambda^{+} \quad = \quad & \min_{\boldsymbol{\epsilon}^{p}_{ki},\,\Delta\mathbf{u},\,\Delta\mathbf{E}} \sum_{i=1}^{\mathcal{N}_L}\sum_{k=1}^{\mathcal{N}_{ed}} \xi_i s_{ki} \\
& \text{s.t} \begin{cases}
\displaystyle\sum_{i=1}^{\mathcal{N}_L}\sum_{k=1}^{\mathcal{N}_{ed}} A_k \boldsymbol{\sigma}^{eT}_{ki}\boldsymbol{\epsilon}^{p}_{ki} = 1 \\
\Delta\boldsymbol{\epsilon}^{h}_{k} = \displaystyle\sum_{i=1}^{\mathcal{N}_L} \boldsymbol{\epsilon}^{p}_{ki} = \tilde{\mathbf{B}}_k \Delta\mathbf{d}, \quad k = 1,\,2,\ldots,\mathcal{N}_{ed} \\
\Delta\mathbf{E} = \dfrac{1}{|\Omega_m|}\displaystyle\sum_{k=1}^{\mathcal{N}_{ed}} A_k \tilde{\mathbf{B}}_k \Delta\mathbf{d} \\
\mathbf{A}_1\Delta\mathbf{d} + \mathbf{A}_2\Delta\mathbf{E} = 0 \\
||\boldsymbol{\chi}_{ki}|| \le s_{ki},\; i = 1,\,2,\ldots,\mathcal{N}_L;\; k = 1,2,\ldots,\mathcal{N}_{ed} \\
\boldsymbol{\chi}_{ki} = \mathbf{J}^{\mathrm{T}}\boldsymbol{\epsilon}^{p}_{ki},\; i = 1,\,2,\ldots,\mathcal{N}_L;\; k = 1,2,\ldots,\mathcal{N}_{ed}
\end{cases}
\end{aligned} \tag{21}$$

The implementation code of the problem (21) is performed within the Matlab environment and the optimisation problem with conic constraint is solved by using the highly efficient solver, Mosek.

5. NUMERICAL EXAMPLE

Circular and rectangular perforated materials are examined in this section. In all examples, the square RVEs of $a \times a$ ($a = 1$ mm) is considered, and under the bi-axial cyclic loads varying independently as

$$\boldsymbol{\Sigma} = \begin{bmatrix} \mu_1 \Sigma_{11} & \mu_2 \Sigma_{22} \end{bmatrix}^{\mathrm{T}}, \; 0 \leq \mu_i \leq 1, \; i = 1, 2 \tag{22}$$

5.1. Circular perforated materials

A thin plate under plane stress condition is considered first. Repeated variable macroscopic stress loads are shown in Fig. 2. Let V_f be the volume fraction.

Fictitious elastic stresses were calculated using the computational homogenisation method presented in [2, 3]. Given elastic parameters are: Young modulus $E = 70$ GPa and Poisson's ratio $\nu = 0.3$. The computed macroscopic strength and fatigue domains of the circular perforated materials for the case when $V_f = 0.3$ and $\alpha = 45^\circ$ are plotted in Fig. 3, and compared with those reported by Carvelli et al. [12] and Maier and Carvelli [4], in which the periodic displacement fields were approximated and a direct iterative optimisation algorithm was used. The effects of the porosity on the macroscopic fatigue criterion are also illustrated Fig. 4.

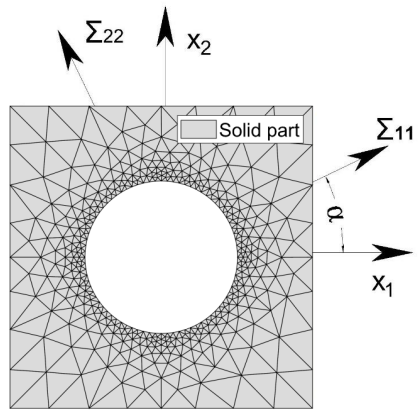

Fig. 2. The RVE of circular perforated materials: geometries, macroscopic stress loads and finite element mesh of 524 nodes and 1,372 edges

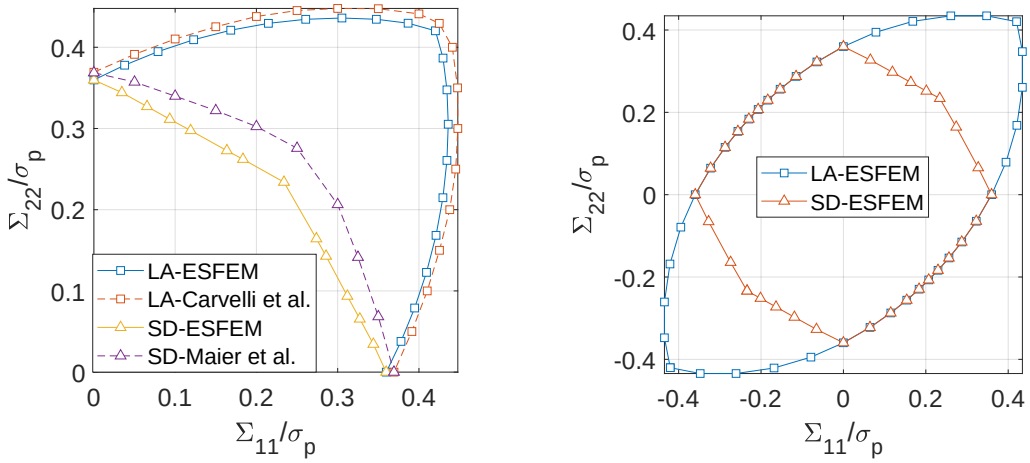

Fig. 3. Circular perforated materials: macroscopic strength (Limit analysis - LA) and fatigue domains (Shakedown - SD) for $V_f = 0.3$ and $\alpha = 45^\circ$

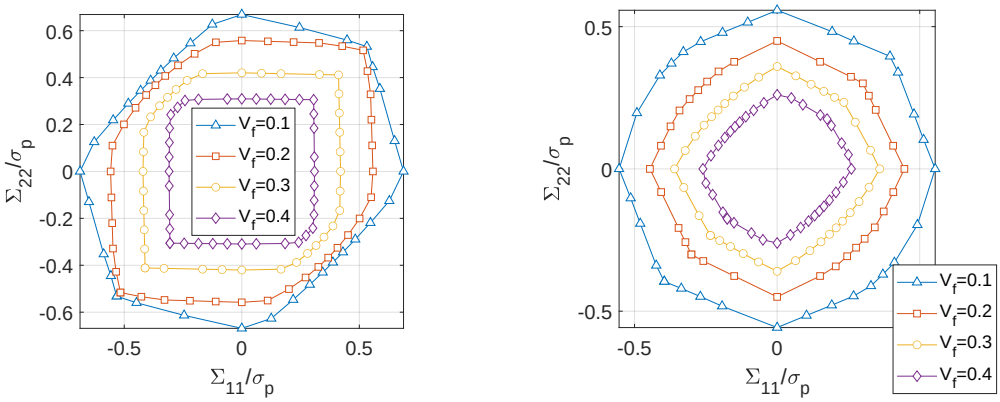

(a) $\alpha = 0^\circ$ (b) $\alpha = 45^\circ$

Fig. 4. Circular perforated materials: the effect of the porosity on the macroscopic fatigue domain

The three dimensional macroscopic fatigue domains of circular perforated materials under three independent macroscopic loads (Σ_{11}, Σ_{22}, Σ_{12}) are plotted in Figs. 5 and 6, where $V_f = 0.3$ and $\alpha = 0^\circ$ or $\alpha = 45^\circ$. The computed values of each domain were obtained by solving 440 optimisation problems of 77,880 variables per each. The computed

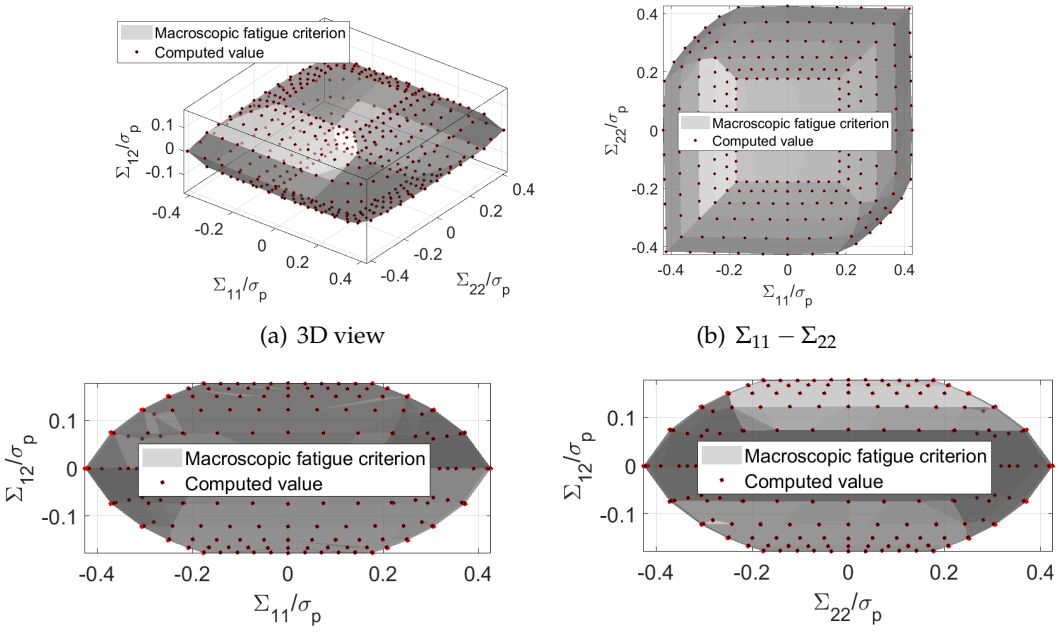

(a) 3D view (b) $\Sigma_{11} - \Sigma_{22}$

(c) $\Sigma_{11} - \Sigma_{12}$ (d) $\Sigma_{22} - \Sigma_{12}$

Fig. 5. Circular perforated materials: macroscopic fatigue domains for $V_f = 0.3$ and $\alpha = 0^\circ$

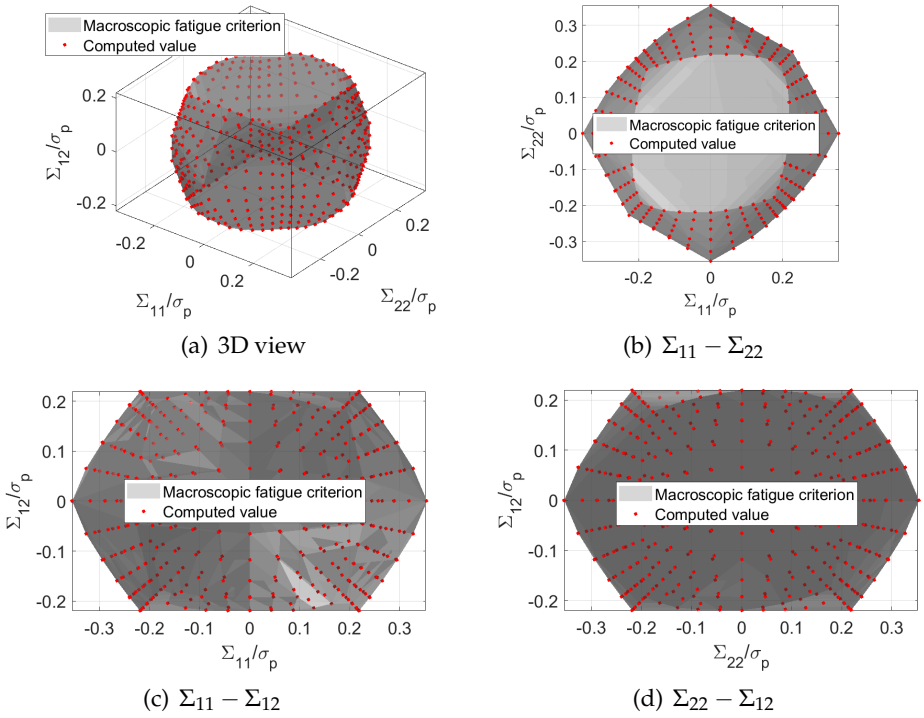

(a) 3D view (b) $\Sigma_{11} - \Sigma_{22}$

(c) $\Sigma_{11} - \Sigma_{12}$ (d) $\Sigma_{22} - \Sigma_{12}$

Fig. 6. Circular perforated materials: macroscopic fatigue domains for $V_f = 0.3$ and $\alpha = 45^\circ$

macroscopic fatigue domains can be fitted in the form of a general quadratic function as

$$\Psi(\boldsymbol{\Sigma}) = \frac{b_1}{\sigma_p^2}\Sigma_{11}^2 + \frac{b_2}{\sigma_p^2}\Sigma_{22}^2 + \frac{b_3}{\sigma_p^2}\Sigma_{11}\Sigma_{22} + \frac{b_4}{\sigma_p^2}\Sigma_{12}^2 + \frac{a_1}{\sigma_p}\Sigma_{11} + \frac{a_2}{\sigma_p}\Sigma_{22} - 1 = 0 \tag{23}$$

where $b_3^2 - 4b_1b_2 < 0$. By means of the least square method, material parameters a_i and b_i can be numerically approximated and reported in Table 1.

Table 1. Circular perforated materials: material parameters of fitted fatigue criteria

Materials	V_f	b_1	b_2	b_3	b_4	a_1	a_2
von Mises ($\alpha = 0^\circ$)	0.1	2.2930	2.3027	−0.6712	8.1464	0.0000	0.0000
	0.2	2.9709	2.9718	−0.9333	14.8425	0.0000	0.0000
	0.3	4.6544	4.6634	−0.8393	26.6311	0.0000	0.0000
	0.4	8.2446	8.2433	−0.3171	54.0049	0.0000	0.0000
von Mises ($\alpha = 45^\circ$)	0.1	3.5582	3.5274	−0.2086	4.0523	0.0000	0.0000
	0.2	6.1697	6.0686	−0.6391	5.9225	0.0000	0.0000
	0.3	10.4769	10.4879	−1.9112	10.3136	0.0000	0.0000
	0.4	19.6536	19.6912	−4.6518	22.0363	0.0000	0.0000

Next, the present solutions are compared with those previously investigated in [13] using both kinematic and static limit analysis. To this end, the computed macroscopic domains are mapped into the plane involving the average hydro-static stress Σ_m and a macroscopic stress Σ_{cp}, defined by

$$\Sigma_m = \frac{\Sigma_{11} + \Sigma_{22}}{2}, \quad \Sigma_{cp} = \frac{\sqrt{3}(\Sigma_{11} - \Sigma_{22})}{2} \tag{24}$$

Fig. 7 illustrates the present computed domains with those reported in [13, 14]. The present strength domains are not matched with those of [13] using finite element method. This may be due to the fact that different types of boundary conditions are applied in the two formulations, i.e. the periodic conditions ($\tilde{\mathbf{u}} = \mathbf{u} - \mathbf{E} \cdot \mathbf{x}$ periodic on boundary of RVE) in the present approach and the uniform strain boundary conditions ($\tilde{\mathbf{u}} = 0$ on boundary of RVE) in [13].

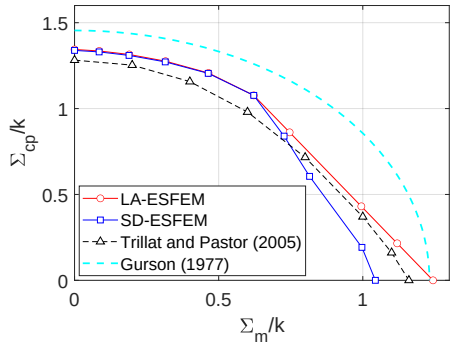

Fig. 7. Circular perforated materials: the mapped domains in comparison with others in case of $V_f = 0.16$

5.2. Rectangular perforated materials

Finally, an RVE with a rectangular hole ($L_1 \times L_2$) at its center, as shown in Fig. 8 is considered. The matrix of the rectangular perforated RVE is aluminium *Al* with yield stress $\sigma_p = 137$ MPa and obeyed von Mises criterion.

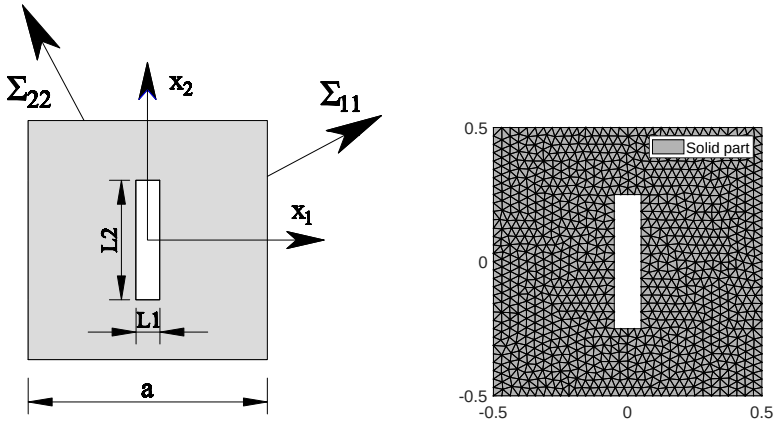

Fig. 8. The rectangular perforated RVE: geometry and mesh of 1041 nodes and 2955 edges

The effects of the hole's shape on fatigue and strength domains are shown in Fig. 9 in the plane of macro principal stress ($\Sigma_{11} - \Sigma_{22}$). When considering macro shear stress Σ_{12} the effects of the hole's shape on the three-dimensional fatigue domains are shown in Fig. 10. The fitted functions of the computed fatigue domains for rectangular perforated material are reported in Table 2.

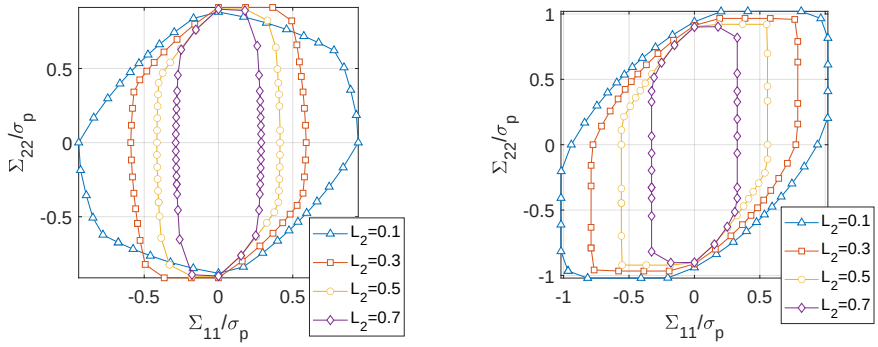

(a) Fatigue domain (b) Strength domain

Fig. 9. Rectangular perforated materials: macroscopic strength domain and fatigue domain with $L_1 = 0.1$

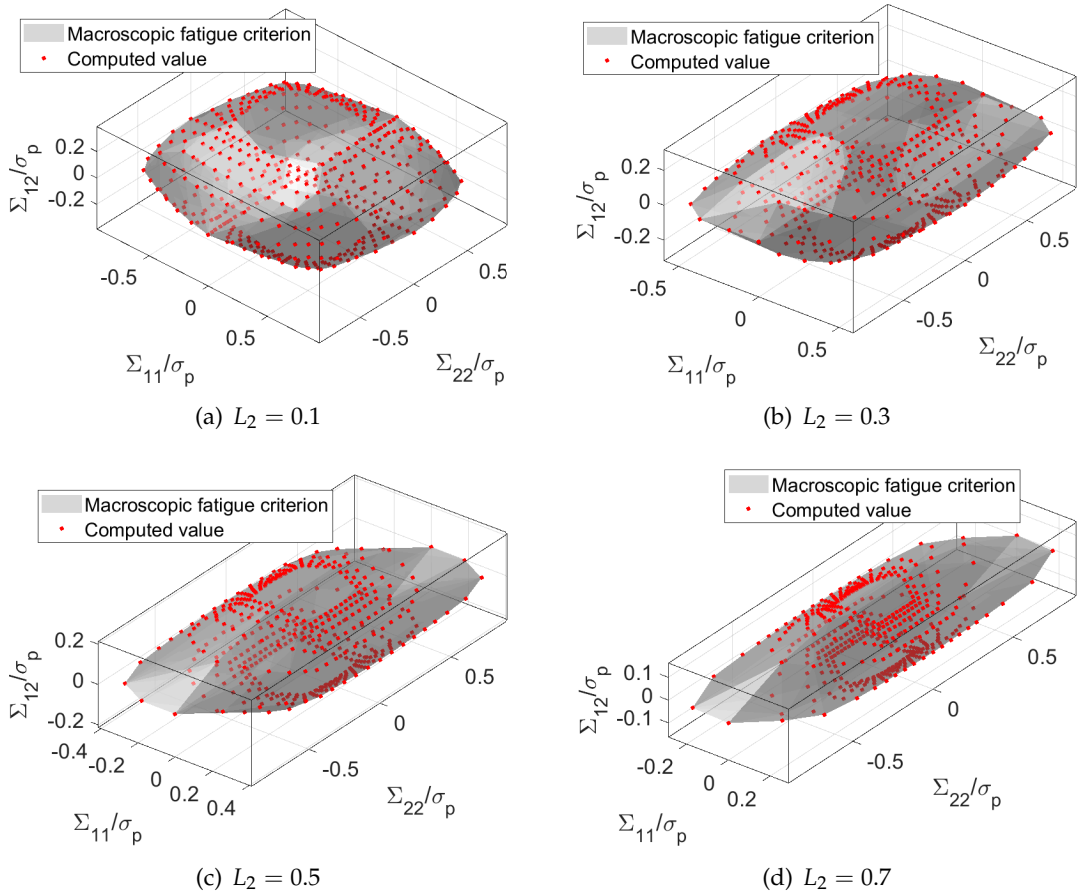

(a) $L_2 = 0.1$ (b) $L_2 = 0.3$

(c) $L_2 = 0.5$ (d) $L_2 = 0.7$

Fig. 10. Rectangular perforated materials: three dimensional fatigue domains with $L_1 = 0.1$

Table 2. Rectangular perforated materials: material parameters of fitted fatigue criteria

Materials	L_2	b_1	b_2	b_3	b_4	a_1	a_2
von Mises ($\alpha = 0^\circ$)	0.1	1.2691	1.6297	−0.2945	6.2576	0.0000	0.0000
	0.3	3.6236	1.0311	−0.2987	11.6711	0.0000	0.0000
	0.5	7.0256	1.1769	−0.4207	26.6209	0.0000	0.0000
	0.7	16.6706	0.7398	−0.2296	53.5227	0.0000	0.0000

6. CONCLUSION

A computational procedure, that uses the edge-based smoothed finite element method in combination with the homogenisation theory and kinematic shakedown theorem, for the estimation of the macroscopic strength and fatigue domains of periodic perforated materials is described. Numerical examples are performed to show the effects of the hole's shape and size on the macroscopic strength and fatigue domains. Moreover, the present numerical method based on the ES-FEM can result in more accurate solutions than that of using the FEM reported in the literature. The method can be further developed for the problems with higher dimension, more complex yield conditions and random voids, which is the subject of future research.

ACKNOWLEDGMENT

This research has been supported by the Vietnam National Foundation for Science and Technology Development (NAFOSTED) under grant number 107.02-2018.31.

REFERENCES

[1] R. J. M. Smit, W. A. M. Brekelmans, and H. E. H. Meijer. Prediction of the mechanical behavior of nonlinear heterogeneous systems by multi-level finite element modeling. *Computer Methods in Applied Mechanics and Engineering*, **155**, (1-2), (1998), pp. 181–192. https://doi.org/10.1016/s0045-7825(97)00139-4.

[2] V. Kouznetsova, W. A. M. Brekelmans, and F. P. T. Baaijens. An approach to micro-macro modeling of heterogeneous materials. *Computational Mechanics*, **27**, (2001), pp. 37–48. https://doi.org/10.1007/s004660000212.

[3] M. G. D. Geers, V. G. Kouznetsova, and W. A. M. Brekelmans. Multi-scale computational homogenization: Trends and challenges. *Journal of Computational and Applied Mathematics*, **234**, (2010), pp. 2175–2182. https://doi.org/10.1016/j.cam.2009.08.077.

[4] G. Maier and V. Carvelli. A kinematic method for shakedown and limit analysis of periodic heterogeneous media. In *Inelastic Behaviour of Structures under Variable Repeated Loads*, pp. 115–132. Springer, (2002). https://doi.org/10.1007/978-3-7091-2558-8_7.

[5] V. Carvelli. Shakedown analysis of unidirectional fiber reinforced metal matrix composites. *Computational Materials Science*, **31**, (1-2), (2004), pp. 24–32. https://doi.org/10.1016/j.commatsci.2004.01.030.

[6] H. X. Li. Kinematic shakedown analysis of anisotropic heterogeneous materials: a homogenization approach. *Journal of Applied Mechanics*, **79**, (2012). https://doi.org/10.1115/1.4006056.

[7] H. X. Li. A microscopic nonlinear programming approach to shakedown analysis of cohesive–frictional composites. *Composites Part B: Engineering*, **50**, (2013), pp. 32–43. https://doi.org/10.1016/j.compositesb.2013.01.018.

[8] J. A. König. *Shakedown of elastic-plastic structures*. Elsevier, (2012).

[9] G. R. Liu, T. Nguyen-Thoi, and K. Y. Lam. An edge-based smoothed finite element method (ES-FEM) for static, free and forced vibration analyses of solids. *Journal of Sound and Vibration*, **320**, (2009), pp. 1100–1130. https://doi.org/10.1016/j.jsv.2008.08.027.

[10] C. V. Le, H. Nguyen-Xuan, H. Askes, and T. Nguyen-Thoi. Computation of limit load using edge-based smoothed finite element method and second-order cone programming. *International Journal of Computational Methods*, **10**, (2013). https://doi.org/10.1142/s0219876213400045.

[11] C. V. Le, P. H. Nguyen, H. Askes, and C. D. Pham. A computational homogenization approach for limit analysis of heterogeneous materials. *International Journal for Numerical Methods in Engineering*, **112**, (10), (2017), pp. 1381–1401. https://doi.org/10.1002/nme.5561.

[12] V. Carvelli, G. Maier, and A. Taliercio. Kinematic limit analysis of periodic heterogeneous media. *Computer Modeling in Engineering and Sciences*, **1**, (2), (2000), pp. 19–30.

[13] M. Trillat and J. Pastor. Limit analysis and Gurson's model. *European Journal of Mechanics-A/Solids*, **24**, (5), (2005), pp. 800–819. https://doi.org/10.1016/j.euromechsol.2005.06.003.

[14] A. L. Gurson. Continuum theory of ductile rupture by void nucleation and growth: Part I—yield criteria and flow rules for porous ductile media. *Journal of Engineering Materials and Technology*, **99**, (1977), pp. 2–15. https://doi.org/10.1115/1.3443401.